NUCL SCI TECH (2021) 32:7
https://doi.org/10.1007/s41365-020-00840-4

Extraction of inclusive photon production at mid-rapidity in $p + p$ and Au + Au collisions at $\sqrt{s_{\rm NN}}$ = 200 GeV

Sheng-Hui Zhang[1,2] · Rong-Rong Ma[3] · Yi-Fei Zhang[1] · Xiao-Long Chen[1] · Xiu-Jun Li[1] · Fan Si[1] · Cheng Li[1] · Ming Shao[1] · Yong-Jie Sun[1] · Ze-Bo Tang[1] · Wang-Mei Zha[1]

Received: 26 October 2020 / Revised: 30 November 2020 / Accepted: 1 December 2020 / Published online: 19 January 2021

Abstract We present a comprehensive study on the individual sources of an inclusive photon production during high-energy hadronic collisions. The cross section and invariant yields of inclusive photons are obtained as a function of $p_{\rm T}$ at mid-rapidity ($|y| < 0.5$) in $p + p$ and Au + Au collisions at $\sqrt{s_{\rm NN}}$ = 200 GeV, respectively. These results provide crucial inputs to separate measurements of open bottom and charm hadron yield suppression in heavy-ion collisions, which are used to test the mass hierarchy of the parton energy loss in the quark gluon plasma created during these collisions. The procedure developed in this study can also be applied to other measurements of electrons from an open heavy-flavor hadron decay, such as the collective flow in the RHIC beam energy scan program.

Keywords Inclusive photon · Cross section · Invariant yields · Mass hierarchy · Technical reference

This work was supported by National Key Research and Development Program of China (Nos. 2018YFE0205200, 2018YFE0104700, and 2020YFE0202002), National Natural Science Foundation of China (No. 11890712), Natural Science Foundation of Anhui Province (No. 1808085J02), Fundamental Research Funds for the Central Universities (No. WK2030000013) and the Project funded by the China Postdoctoral Science Foundation (No. 2019M652177).

✉ Yi-Fei Zhang
ephy@ustc.edu.cn

1 University of Science and Technology of China, Hefei 230026, China

2 University of Illinois at Chicago, Chicago, IL 60607, USA

3 Brookhaven National Laboratory, Upton, NY 11973, USA

1 Introduction

Searching for a novel form of nuclear matter with deconfined quarks and gluons, created during ultra-relativistic heavy-ion collisions, is one of the main goals of high-energy nuclear physics. Many measurements from the Relativistic Heavy Ion Collider (RHIC) and the Large Hadron Collider (LHC) experiments show that this strongly coupled matter, usually referred to as quark-gluon plasma (QGP), have indeed been formed [1–4]. The next step is to study its properties in detail.

Heavy quarks (c and b) are predominantly produced during the early stages of heavy-ion collisions before the creation of the QGP [5, 6]. They subsequently traverse the QGP throughout its evolution and thus can serve as an excellent probe for studying the properties of the QGP. Heavy flavor quarks are expected to suffer from collisional and radiative energy losses through interactions with the QGP. The nuclear modification factor ($R_{\rm AA}$) is utilized to quantify such energy loss by comparing the yields of open heavy flavor production in heavy-ion collisions with those during $p + p$ collisions. Significant suppression of the charm meson yielded at large transverse momenta ($p_{\rm T}$), resulting from the substantial energy loss of heavy quarks in the QGP, has been observed at both the RHIC and LHC [7–12], indicating strong interactions between heavy quarks and the medium. This energy loss is expected to be different for bottom and charm quarks owing to their different masses [13]. Separate measurements of open bottom and open charm hadron production during heavy-ion collisions are crucial to testing the mass hierarchy of the parton energy loss in the QGP.

For open bottom hadron production at RHIC, they are only measured indirectly through their decay products, such as electrons, J/Ψ, and D^0, owing to the low production rates and small branching ratios for the hadronic decay channels. Measurements of R_{AA} for J/Ψ and D^0 from open bottom hadron decay are currently limited owing to a lack of reference measurements during $p+p$ collisions [14]. By contrast, owing to their relatively large branching ratios, the R_{AA} of the electrons from open bottom and charm hadron decay can be obtained separately using the following ingredients: (1) R_{AA} of inclusive heavy-flavor electrons (HFEs) from open bottom and charm hadron decay, (2) the contribution of open bottom hadron decay to HFE in 200 GeV $p+p$ collisions measured through azimuthal correlations between HFEs and associated hadrons [15], (3) the contribution of open bottom hadron decay to HFEs in Au + Au collisions at $\sqrt{s_{\mathrm{NN}}}$ = 200 GeV with displaced vertices or a data driven technique [16] making use of the precise measurement of displaced vertices from the Heavy Flavor Tracker (HFT) [17] at the Solenoidal Tracker At RHIC (STAR).

In the measurements of HFE spectra in $p+p$ and Au + Au collisions, the HFE sample can be obtained by statistically subtracting the background photonic electrons from the inclusive electron sample. Photonic electrons arise from Dalitz decay of light-neutral mesons and photon conversions in the detector material. Owing to the extremely low signal-to-background ratio, it is crucial to extract the background electron yields and kinematic distributions accurately for precise measurements of HFE spectra. Furthermore, the contribution of the open bottom hadron decays to the HFE sample in Au + Au collisions is obtained through a template fitting to the distribution of the distance of the closest approach (DCA) to the collision vertex for inclusive electrons [14]. Contributions from photonic electrons are included in the templates. Another important observation is the charm angular correlation, which is believed to be a sensitive probe of the medium dynamics during the early stage of the collisions [18]. Measurements of the charm angular correlation when reconstructing the open charm mesons are extremely challenging, and an indirect measurement of the correlation between their decay electrons requires inclusive photon yields as well. However, it is difficult to directly measure the inclusive photon spectrum experimentally, and a cocktail-like method is usually applied.

In this paper, we report an indirect measurement of inclusive photon spectra as a function of p_{T} at mid-rapidity ($|y|<0.5$) in $p+p$ collisions and different centrality classes of Au+Au collisions at $\sqrt{s_{\mathrm{NN}}}$ = 200 GeV. There are five main sources of photon production: π^0 and η two-body decays, π^0 and η Dalitz decays, and direct photons. Direct photon distributions were obtained based on the available measurements and an extrapolation. Photons from π^0 and η decay are extracted using PYTHIA for decay kinematics with measured π^0 and η distributions as inputs. In previous studies [19], the rapidity distributions for π^0 and η are assumed to be flat, whereas more realistic shapes are used in this work. In addition, contributions from π^0 and η Dalitz decays to the inclusive photon production are taken into account, which were omitted in previous studies.

The paper is organized as follows: PYTHIA settings, cross section, and invariant yields as a function of p_{T} for inclusive photons in $p+p$ and Au + Au collisions are presented in Sect. 2. A summary is given in Sect. 3.

2 Results

2.1 PYTHIA decay process

PYTHIA is an event generator widely used in high-energy particle and nuclear physics communities [20]. In this study, PYTHIA6.319 was used to decay π^0 and η mesons into photons through both two-photon and Dalitz decay channels for both p+p and Au+Au collisions. The p_{T} and rapidity distributions of π^0 and η mesons are obtained from experimental measurements. Information on daughter particles was stored for further analysis.

2.2 p+p Collisions at $\sqrt{s}$ = 200 GeV

The four momenta of parent particles (π^0 and η) are input to PYTHIA for decay into photons. The measured π^0 cross section at mid-rapidity ($|\eta|<0.35$) from the PHENIX collaboration [21–23] and calculated π^0 ($(\pi^+ + \pi^-)/2$) cross section at mid-rapidity ($|y|<0.1$ and $|y|<0.5$) from the STAR collaboration [24–28] during $p+p$ collisions at $\sqrt{s}$ = 200 GeV are shown inFig. 1a. The η meson cross section was measured at mid-rapidity by both STAR ($|y|<0.5$ and $0<\eta<1$) and PHENIX ($|\eta|<0.35$) collaborations [21, 29–31], as shown in Fig. 1a. Their cross sections as a function of p_{T}, assumed to have a similar shape in different mid-rapidity intervals, are parameterized using the Tsallis statistics

$$E\frac{\mathrm{d}^3N}{\mathrm{d}p^3} = C_n m_{\mathrm{T}}\left(1+(q-1)\frac{m_{\mathrm{T}}}{T}\right)^{-1/(q-1)}, \tag{1}$$

where $m_{\mathrm{T}}=\sqrt{(p_{\mathrm{T}}^2+m^2)}$, m is the particle mass, and C_n, q, and T are free parameters. The fitting results, shown as solid lines in Fig. 1a, are used as inputs. The input rapidity distributions of π^0 and η are parameterized based on Landau hydrodynamics, with a Gaussian-like function $\cosh^{-2}\left(\frac{3y}{4\sigma_{\mathrm{Landau}}\left(1-\frac{y^2}{2\sqrt{s}/m}\right)}\right)$, where $\sigma_{\mathrm{Landau}}=$

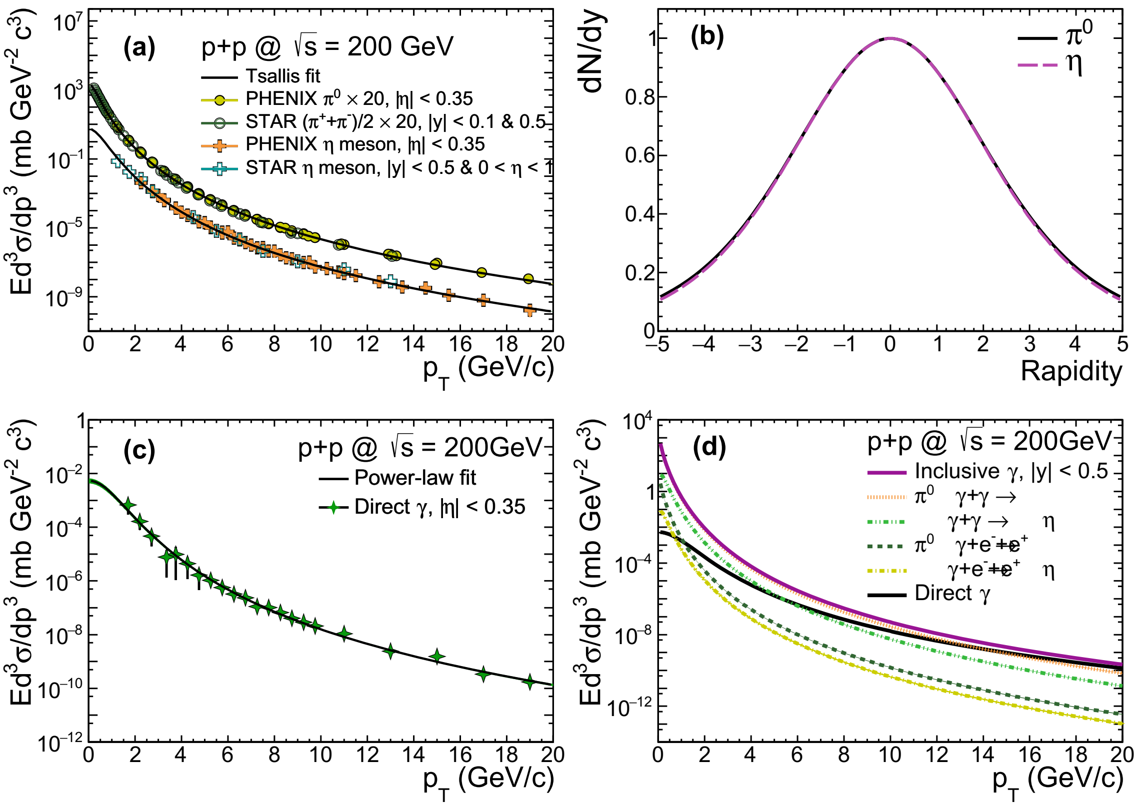

Fig. 1 **a** Cross sections as a function of p_T for π^0, $(\pi^+ + \pi^-)/2$, and η mesons at mid-rapidity in p+p collisions at $\sqrt{s}$ = 200 GeV measured using STAR and PHENIX [21–27, 29–31]. Error bars indicate point-to-point uncertainties. Solid lines represent the Tsallis function fits. The error bands depict parameterization uncertainties. **b** Parameterization of *dN/dy* as a function of rapidity for π^0 and η mesons [32, 33]. **c** Direct photon cross section as a function of p_T measured by PHENIX [34–36] along with a power-law fit at mid-rapidity in $p + p$ collisions at $\sqrt{s}$ = 200 GeV. Error bars denote point-to-point uncertainties. The error band shows the parameterization uncertainty. **d** Inclusive photon cross section as a function of p_T at mid-rapidity ($|y| < 0.5$) in $p + p$ collisions at $\sqrt{s}$ = 200 GeV. Different photon sources are also shown. Bands represent uncertainties, including those from parameterization and branching ratios. A global uncertainty of 8% is not shown. Owing to the large y-axis scale, the error bands are difficult to see given the small relative errors. The same is shown in the following figures

$\sqrt{\ln(\sqrt{s}/(2m_N))}$, $\sqrt{s}$ is the nucleon-nucleon center of mass energy, m is the particle mass, and m_N is a nucleon mass [32, 33]. These are shown in Fig. 1b.

The parent particle production is isotropic in azimuth, and therefore, their azimuthal angle (ϕ) distributions are sampled uniformly within the $0 \sim 2\pi$ range. With the input distributions extracted, the p_T distributions of photons from π^0 and η decay are obtained using PYTHIA and normalized based on the branching ratio of $\pi^0/\eta \rightarrow e^+e^-\gamma/\gamma\gamma$ and π^0/η dN/dy. The p_T distributions of the decayed photons are shown in Fig. 1d.

In addition, the direct photon contribution is based on the PHENIX measurement of the direct photon cross section as a function of p_T during 200 GeV $p + p$ collisions at mid-rapidity ($|\eta| < 0.35$), fitted using a power-law function $a(1 + \frac{p_T^2}{b})^c$, where a, b, and c are free parameters [34–36]. The data points and the fit curve are shown in Fig. 1c. The inclusive photon cross section is obtained by summing π^0 and η meson decayed and direct photons, as shown in Fig. 1d.

2.3 Au + Au Collisions at $\sqrt{s_{NN}}$ = 200 GeV

The inclusive photon invariant yields at mid-rapidity in Au + Au collisions at $\sqrt{s_{NN}}$ = 200 GeV are obtained using a similar approach as for $p + p$ collisions described in Sect. 2.2. One notable difference is that the π^0 and η production yields and p_T distributions are modified in the QGP mainly owing to the collective flow and paton energy loss. In addition to the contributions from the initial hard scatterings and jet fragmentation to the direct photon production, the thermal photon radiation, mainly from the partonic phase of the medium created during heavy-ion collisions, is also included in this category.

The invariant yields of π^0 as a function of p_T, inferred from the STAR measurement ($(\pi^+ + \pi^-)/2$, $|y| < 0.5$) [37] and directly measured through the PHENIX experiment

($|y|<0.35$) [38, 39], are shown in Fig. 2a for Au + Au collisions of different centrality classes. Good agreements are seen among the different measurements in the overlapping kinematic range. Because of in-medium modifications of these yields compared to those in $p + p$ collisions [40], the modified Tsallis function is used to fit the $p_{\rm T}$ spectra:

$$E\frac{{\rm d}^3N}{{\rm d}p^3} = A_1\left[\exp\left(-\frac{\beta p_{\rm T}}{p_1}\right)+\frac{m_{\rm T}}{p_1}\right]^{-n_1} : p_{\rm T} < p_{\rm Tth},$$
$$E\frac{{\rm d}^3N}{{\rm d}p^3} = A_2\left[\frac{B}{p_2}\left(\frac{p_{\rm T}}{q_0}\right)^{\alpha}+\frac{m_{\rm T}}{p_2}\right]^{-n_2} : p_{\rm T} > p_{\rm Tth}, \quad (2)$$

where A_1, β, p_1, n_1, A_2, B, p_2, q_0, and n_2 are free parameters. This function takes into account the thermal production and collective effects at a low $p_{\rm T}$ and the parton energy loss effect at a high $p_{\rm T}$ [40]. We found that this function can describe well the π^0 spectra with $p_{\rm Tth} = 7$ GeV/c. The fitting results are also shown in Fig. 2a as solid curves. The error bands arise from point-to-point uncertainties in the data. The rapidity distribution for π^0 is assumed to be the same as that in the $p + p$ collisions, as shown in Fig. 1b.

Because of the limited precision and kinematic coverage by the available measurements of η meson invariant yields, the $p_{\rm T}$ spectrum shape is obtained by utilizing the m_T scaling method [19], that is, taking the parameterized $p_{\rm T}$ spectrum shape for π^0 (Fig. 2a) and replacing its $p_{\rm T}$ with $\sqrt{p_{\rm T}^2 + m_\eta^2 - m_{\pi^0}^2}$. To obtain the absolute normalization, the yield ratios of η to π^0 from measurements [31] are $0.4 \pm 0.04({\rm stat}) \pm 0.02({\rm sys})$, with no strong $p_{\rm T}$ or centrality dependencies observed. This ratio is used to fix the normalization for η meson-invariant yields in all centrality bins, shown as the solid bands in Fig. 2b. Also shown in Fig. 2b are the measurements of η meson-invariant yields at mid-rapidity ($|\eta|<0.35$) [41], which are seen to agree spectra quite well with the parameterized $p_{\rm T}$. As a consistent check, this method is also applied to $p + p$ collisions, and the result from $m_{\rm T}$ scaling for η meson is seen to agree with the experimental measurement down to 1 GeV/c. Similar to the case of π^0, the rapidity distribution of the η meson is also assumed to be the same as that during $p + p$ collisions, as shown in Fig. 1b.

Invariant yields of direct photons at mid-rapidity ($|y|<1$) in different centralities of 200 GeV Au+Au collisions were measured using the STAR experiment [42], as shown in Fig. 3a. They are fitted with an exponential function plus the fit to the corresponding distribution in $p + p$ collisions scaled by $N_{\rm coll}$ [43], that is, $Ae^{-p_{\rm T}/T} + N_{\rm coll} \times A_{pp}(1 + {p_{\rm T}}^2/b)^{-n}$, where A, T, A_{pp}, b, and n are free parameters, and $N_{\rm coll}$ is the number of binary nucleon-nucleon collisions in different Au + Au centrality classes. The first term is used to describe the thermal photon radiation, whereas the second term is motivated by the fact that photons do not interact strongly with the QGP and thus do not exhibit a spectrum modification compared to the $p + p$ collisions. To obtain the direct photon yields in 0–10% and 10–20% centralities that are not measured, the following extrapolation procedure [25] is used:

- Obtain ${\rm d}N/{\rm d}y/\langle 0.5N_{\rm part}\rangle$ as a function of $N_{\rm part}$, where ${\rm d}N/{\rm d}y$ is the integrated direct photon yield based on the

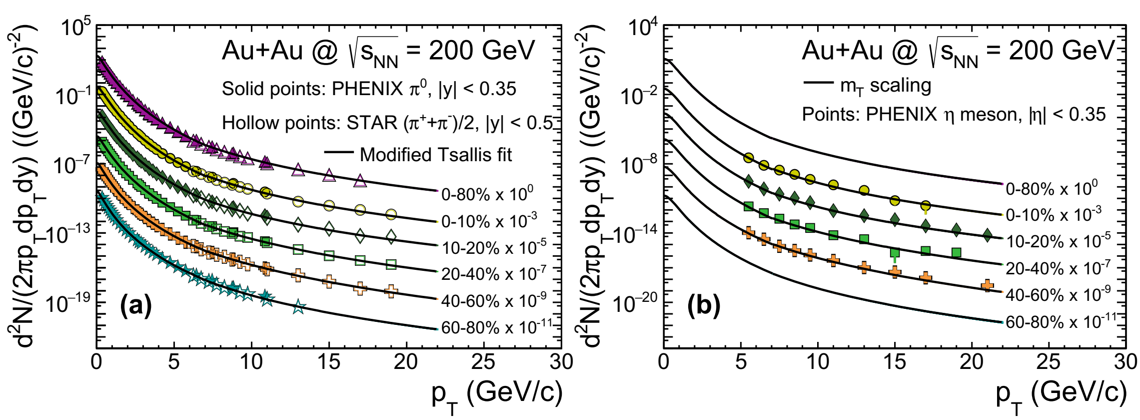

Fig. 2 **a** Invariant yields of π^0 and $(\pi^+ + \pi^-)/2$ as a function of $p_{\rm T}$ at mid-rapidity for different centrality classes in Au + Au collisions at $\sqrt{s_{\rm NN}}$ = 200 GeV measured by STAR and PHENIX [37–39]. Error bars indicate point-to-point uncertainties. Solid lines represent modified Tsallis function fits. The error bands depict parameterization uncertainties. **b** Invariant yields of η mesons as a function of $p_{\rm T}$ at mid-rapidity, shown as solid symbols, for 0–10%, 10–20%, 20–40%, and 40–60% Au + Au collisions at $\sqrt{s_{\rm NN}}$ = 200 GeV as measured by PHENIX [41]. Error bars on the data points denote point-to-point uncertainties. The shaded bands represent parameterized η meson yields in various centrality classes based on $m_{\rm T}$ scaling of parameterized π^0 $p_{\rm T}$ spectra and the measured η to π^0 yield ratio. The spread of the shaded bands arises from the uncertainties in parameterizing the measured π^0 yields, as shown in the left panel, and the error in the η to π^0 yield ratio

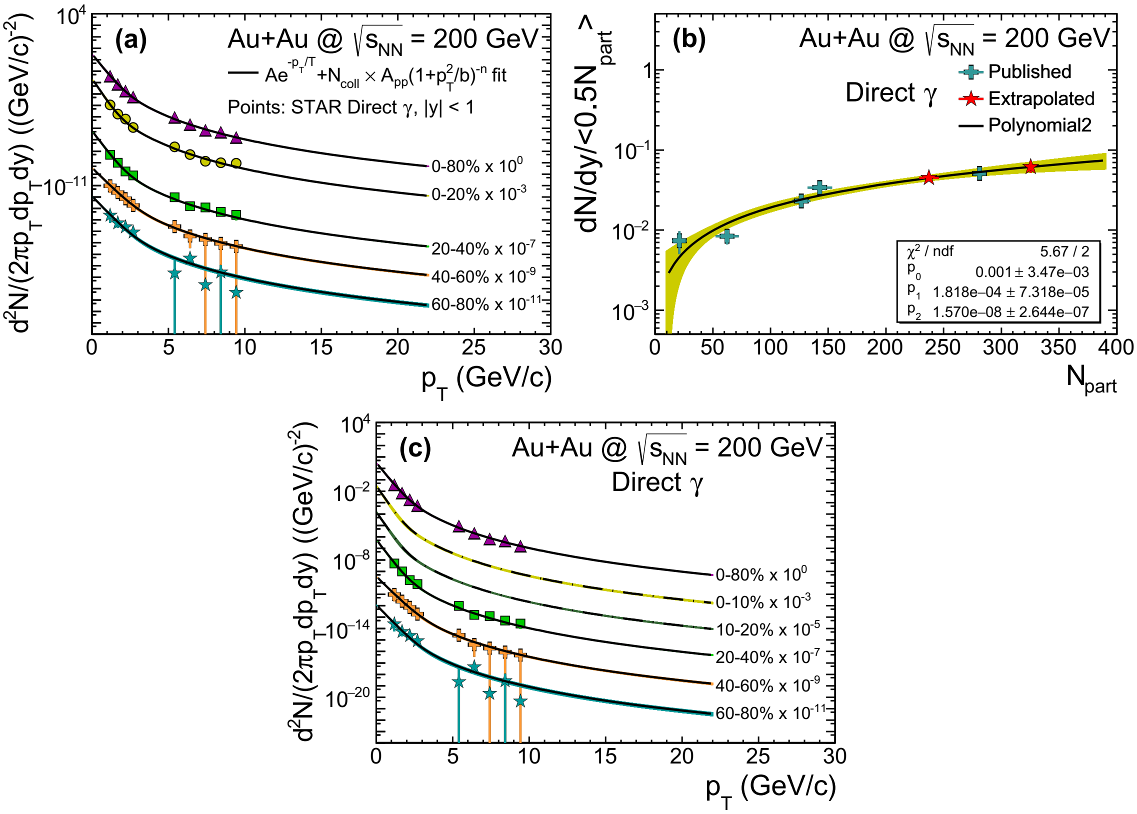

Fig. 3 **a** Invariant yields of direct photons as a function of p_T at mid-rapidity ($|y| < 1$) for different centrality classes in Au + Au collisions at $\sqrt{s_{NN}}$ = 200 GeV as measured using STAR [42]. Error bars indicate point-to-point uncertainties. Solid lines represent fits to the data points with an exponential function plus the fit to the corresponding distribution measured during $p + p$ collisions scaled by N_{coll}. Error bands depict uncertainties in the parameterization and N_{coll}. **b** Direct photon $dN/dy/\langle 0.5N_{part}\rangle$ as a function of N_{part} along with a fit utilizing the second-order polynomial function. Error bars denote point-to-point uncertainties, and the error band shows the parameterization uncertainty. **c** Direct photon invariant yields as a function of p_T from measurements and extrapolation for different centrality classes of Au+Au collisions. For the 0–10% and 10–20% centrality classes, the error bands show uncertainties from extrapolated inclusive direct photon yields, N_{part} values, and parameterization of the direct photon p_T spectrum in the 0–20% centrality bin

fit to the measured spectrum, and N_{part} is the number of participating nucleons in each centrality class.

- Fit $dN/dy/\langle 0.5N_{part}\rangle$ versus N_{part} with a second-order polynomial function, and extrapolate the inclusive direct photon yields in desired centrality bins. Such a distribution and the fit are shown in Fig. 3b.
- The shapes of the invariant yields for direct photons in 0–10% and 10–20% centrality bins are taken to be the same as that of the 0–20% centrality class, as shown in Fig. 3a. Normalization is based on the extrapolated inclusive direct photon yields.

The resulting invariant yields of direct photons in 0–10% and 10–20% centrality bins are shown in Fig. 3c as dash-dotted curves.

With all ingredients in hand, invariant yields of inclusive photons are obtained with contributions from π^0 and η two-body and Dalitz decays, and direct photon production. These are shown as solid curves in Fig. 4 with different panels corresponding to different centrality classes. The dashed and dotted lines represent individual sources. The integrated IPT yields per unit rapidity at mid-rapidity for different centrality classes are summarized in Table 1, along with those from each component. The contribution from π^0 two-body decay is the dominant source of photon production at low p_T, whereas the contribution from direct photon production increases with increasing p_T and overtakes that from π^0 two-body decay at high p_T. In all cases, the neutral meson Dalitz decays constitute less than 1% of inclusive photons within the entire kinematic range.

3 Summary

The inclusive photon cross section and invariant yields as a function of p_T at mid-rapidity ($|y| < 0.5$) were extracted for $p + p$ and Au + Au collisions at $\sqrt{s_{NN}}$ = 200 GeV, respectively. The results provide necessary inputs for subtracting the photonic electron background in measuring

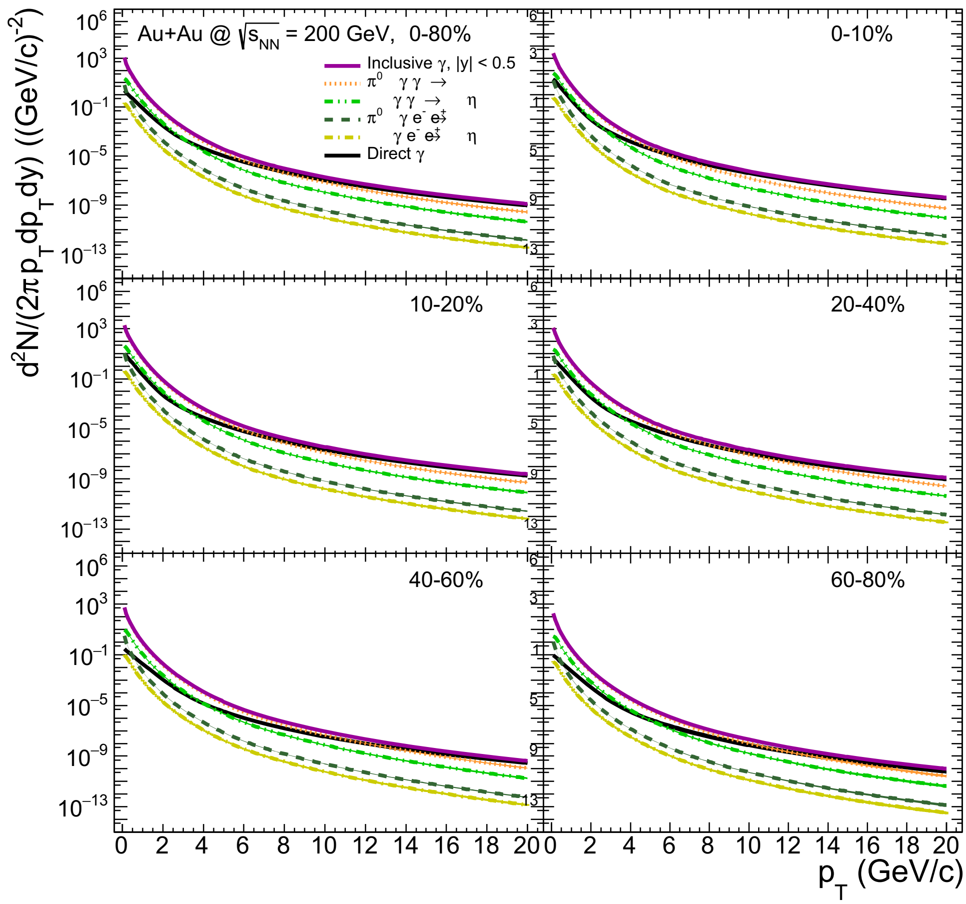

Fig. 4 Invariant yields of inclusive photons as a function of p_T, along with those from different sources, at mid-rapidity ($|y| < 0.5$) for different centrality classes in Au + Au collisions at $\sqrt{s_{NN}}$ = 200 GeV. Error bands on the solid curves include uncertainties from the parameterized π^0, η, and direct photon yields as well as the branching ratios of π^0 and η decaying into photons

Table 1 dN/dy at mid-rapidity for inclusive photon production and individual sources in different centrality classes

Centrality (%)	Inclusive γ	$\pi^0 \to \gamma\gamma$	$\eta \to \gamma\gamma$	$\pi^0 \to e^+e^-\gamma$	$\eta \to e^+e^-\gamma$	Direct γ
0–80	211.631 ± 5.738	199.111 ± 5.446	9.790 ± 1.128	1.182 ± 0.049	0.086 ± 0.011	1.463 ± 0.164
0–10	531.632 ± 14.465	492.109 ± 13.231	26.346 ± 3.040	2.922 ± 0.119	0.230 ± 0.030	10.025 ± 2.318
10–20	382.744 ± 10.274	356.553 ± 9.598	18.599 ± 2.144	2.117 ± 0.086	0.163 ± 0.021	5.313 ± 1.022
20–40	231.482 ± 6.336	217.013 ± 5.998	10.672 ± 1.231	1.288 ± 0.053	0.093 ± 0.012	2.415 ± 0.242
40–60	98.370 ± 3.104	93.218 ± 2.996	4.299 ± 0.499	0.553 ± 0.025	0.038 ± 0.005	0.262 ± 0.035
60–80	32.077 ± 0.739	30.476 ± 0.702	1.331 ± 0.152	0.181 ± 0.007	0.012 ± 0.001	0.078 ± 0.010

HFE yields during both $p + p$ and Au + Au collisions. They also constitute an important component for extracting the fraction of bottom hadron decayed electrons in the HFE sample through template fitting during Au + Au collisions. To test the mass hierarchy of the parton energy loss in the QGP, these measurements are necessary ingredients for calculating R_{AA} of electrons from the bottom and charm hadron decays separately. Furthermore, to study the fundamental properties of the QPG at lower collision energies, the presented procedure provides a technical reference for similar topics in the field, such as a measurement of the HFE elliptic flow [44] in the RHIC beam energy scan II program [45].

Author contributions All authors contributed to the study conception and design. Material preparation, data collection and analysis were performed by Sheng-Hui Zhang. The first draft of the manuscript was written by Sheng-Hui Zhang and all authors commented on previous versions of the manuscript. All authors read and approved the final manuscript.

References

1. S. Edward, Strongly coupled quark-gluon plasma in heavy ion collisions. Rev. Mod. Phys. **89**, 035001 (2017). https://doi.org/10.1103/RevModPhys.89.035001
2. J. Adams, M.M. Aggarwal, Z. Ahammed et al., (STAR Collaboration), Experimental and theoretical challenges in the search for the quark gluon plasma: the STAR collaboration's critical assessment of the evidence from RHIC collisions. Nucl. Phys. A **757**, 102–183 (2005). https://doi.org/10.1016/j.nuclphysa.2005.03.085
3. K. Adcox, S.S. Adler, S. Afanasiev et al., (PHENIX Collaboration), Formation of dense partonic matter in relativistic nucleusnucleus collisions at RHIC: experimental evaluation by the PHENIX Collaboration. Nucl. Phys. A **757**, 184–283 (2005). https://doi.org/10.1016/j.nuclphysa.2005.03.086
4. B. Muller, J. Schukraft, B. Wyslouch, First results from Pb+Pb collisions at the LHC. Ann. Rev. Nucl. Part Sci. **62**, 361–386 (2012). https://doi.org/10.1146/annurev-nucl-102711-094910
5. Z. Lin, M. Gyulassy, Open charm as a probe of preequilibrium dynamics in nuclear collisions. Phys. Rev. C **51**, 2177 (1995). https://doi.org/10.1103/PhysRevC.51.2177; Erratum: Phys. Rev. C 52, 440 (1995). https://doi.org/10.1103/PhysRevC.52.440
6. M. Cacciari, P. Nason, R. Vogt, QCD predictions for charm and bottom quark production at RHIC. Phys. Rev. Lett. **95**, 122001 (2005). https://doi.org/10.1103/PhysRevLett.95.122001
7. Z. Tang, W. Zha, Y. Zhang, An experimental review of open heavy flavor and quarkonium production at RHIC. Nucl. Sci. Tech. **31**, 81 (2020). https://doi.org/10.1007/s41365-020-00785-8
8. X. Luo, S. Shi, N. Xu et al., A study of the properties of the QCD phase diagram in high-energy nuclear collisions. Particles **2020**(3), 278–307 (2020). https://doi.org/10.3390/particles3020022
9. J. Adam, L. Adamczyk, J.R. Adams et al., (STAR Collaboration), Centrality and transverse momentum dependence of D^0-meson production at mid-rapidity in Au+Au collisions at $\sqrt{s_{\mathrm{NN}}} = 200$ GeV. Phys. Rev. C **99**, 034908 (2019). https://doi.org/10.1103/PhysRevC.99.034908
10. B. Abelev, J. Adam, D. Adamova et al., (ALICE Collaboration), Suppression of high transverse momentum D mesons in central Pb–Pb collisions at $\sqrt{s_{\mathrm{NN}}} = 2.76$ TeV. JHEP **09**, 112 (2012). https://doi.org/10.1007/JHEP09(2012)112
11. J. Adam, D. Adamova, M.M. Aggarwal et al., (ALICE Collaboration), Transverse momentum dependence of D-meson production in Pb–Pb collisions at $\sqrt{s_{\mathrm{NN}}} = 2.76$ TeV. JHEP **03**, 081 (2016). https://doi.org/10.1007/JHEP03(2016)081
12. A.M. Sirunyan, A. Tumasyan, W. Adam et al., (CMS Collaboration), Nuclear modification factor of D^0 mesons in PbPb collisions at $\sqrt{s_{\mathrm{NN}}} = 5.02$ TeV. Phys. Lett. B **782**, 474–496 (2018). https://doi.org/10.1016/j.physletb.2018.05.074
13. A. Buzzatti, M. Gyulassy, Jet flavor tomography of quark gluon plasmas at RHIC and LHC. Phys. Rev. Lett. **108**, 022301 (2012). https://doi.org/10.1103/PhysRevLett.108.022301
14. S. Zhang, Open bottom production in Au+Au collisions at $\sqrt{s_{\mathrm{NN}}} = 200$ GeV with the STAR experiment. Proceedings **10**, 39 (2019). https://doi.org/10.3390/proceedings2019010039
15. M.M. Aggarwal, Z. Ahammed, A.V. Alakhverdyants et al., (STAR Collaboration), Measurement of the bottom quark contribution to nonphotonic electron production in p+p Collisions at $\sqrt{s} = 200$ GeV. Phys. Rev. Lett. **105**, 202301 (2010). https://doi.org/10.1103/PhysRevLett.105.202301
16. F. Si, X. Chen, L. Zhou et al., Charm and beauty isolation from heavy flavor decay electrons in Au+Au collisions at $\sqrt{s_{\mathrm{NN}}} = 200$ GeV at RHIC. Phys. Lett. B **805**, 135465 (2020). https://doi.org/10.1016/j.physletb.2020.135465
17. H. Qiu, STAR heavy flavor tracker. Nucl. Phys. A **931**, 1141–1146 (2014). https://doi.org/10.1016/j.nuclphysa.2014.08.056
18. H. Wang, J.H. Chen, Y.G. Ma et al., Charm hadron azimuthal angular correlations in Au+Au Collisions at $\sqrt{s_{\mathrm{NN}}} = 200$ GeV from parton scatterings. Nucl. Sci. Tech. **30**, 185 (2019). https://doi.org/10.1007/s41365-019-0706-z
19. H. Agakishiev, M.M. Aggarwal, Z. Ahammed et al., (STAR Collaboration), High p_T non-photonic electron production in p+p collisions at $\sqrt{s}$ =200 GeV. Phys. Rev. D **83**, 052006 (2011). https://doi.org/10.1103/PhysRevD.83.052006
20. T. Sjöstrand, S. Mrenna, P. Skands, PYTHIA 6.4 physics and manual. JHEP **0605**, 026 (2006). https://doi.org/10.1088/1126-6708/2006/05/026
21. S.S. Adler, S. Afanasiev, C. Aidala et al., (PHENIX Collaboration), Centrality dependence of π^0 and η production at large transverse momentum in $\sqrt{s_{\mathrm{NN}}} = 200$ GeV d+Au collisions. Phys. Rev. Lett. **98**, 172302 (2007). https://doi.org/10.1103/PhysRevLett.98.172302
22. A. Adare, S. Afanasiev, C. Aidala et al., (PHENIX Collaboration), Inclusive cross section and double helicity asymmetry for π^0 production in p + p collisions at $\sqrt{s} = 200$ GeV: Implications for the polarized gluon distribution in the proton. Phys. Rev. D **76**, 051106 (2007). https://doi.org/10.1103/PhysRevD.76.051106
23. S.S. Adare, S. Afanasiev, C. Aidala et al., (PHENIX Collaboration), Midrapidity neutral-pion production in proton-proton collisions at $\sqrt{s} = 200$ GeV. Phys. Rev. Lett. **91**, 241803 (2003). https://doi.org/10.1103/PhysRevLett.91.241803
24. J. Adams, C. Adler, M.M. Aggarwal et al., (STAR Collaboration), Identified particle distributions in pp and Au+Au collisions at $\sqrt{s_{\mathrm{NN}}} = 200$ GeV. Phys. Rev. Lett. **92**, 112301 (2004). https://doi.org/10.1103/PhysRevLett.92.112301
25. B.I. Abelev, M.M. Aggarwal, Z. Ahammed et al., (STAR Collaboration), Systematic measurements of identified particle spectra in pp, d+Au and Au+Au collisions from STAR. Phys. Rev. C **79**, 034909 (2009). https://doi.org/10.1103/PhysRevC.79.034909
26. J. Adams, M.M. Aggarwal, Z. Ahammed et al., (STAR Collaboration), Pion, kaon, proton and anti-proton transverse momentum distributions from p+p and d+Au collisions at $\sqrt{s_{\mathrm{NN}}} = 200$ GeV. Phys. Lett. B **616**, 8–16 (2005). https://doi.org/10.1016/j.physletb.2005.04.041
27. J. Adams, M.M. Aggarwal, Z. Ahammed et al., (STAR Collaboration), Identified hadron spectra at large transverse momentum in p+p and d+Au collisions at $\sqrt{s_{\mathrm{NN}}} = 200$ GeV. Phys. Lett. B **637**, 161–169 (2006). https://doi.org/10.1016/j.physletb.2006.04.032
28. S.H. Zhang, L. Zhou, Y.F. Zhang et al., Multiplicity dependence of charged particle, ϕ meson, and multi-strange particle productions in p+p collisions at $\sqrt{s} = 200$ GeV from PYTHIA simulation. Nucl. Sci. Tech. **29**, 136 (2018). https://doi.org/10.1007/s41365-018-0469-y
29. A. Adare, S. Afanasiev, C. Aidala et al., (PHENIX Collaboration), Cross section and double helicity asymmetry for η mesons and their comparison to π^0 production in p+p collisions at $\sqrt{s} =$ 200 GeV. Phys. Rev. D **83**, 032001 (2011). https://doi.org/10.1103/PhysRevD.83.032001
30. B.I. Abelev, M.M. Aggarwal, Z. Ahammed et al., (STAR Collaboration), Inclusive π^0, η, and direct photon production at high transverse momentum in p+p and d+Au collisions at $\sqrt{s_{\mathrm{NN}}} = 200$ GeV. Phys. Rev. C **81**, 064904 (2010). https://doi.org/10.1103/PhysRevC.81.064904
31. S.S. Adler, S. Afanasiev, C. Aidala et al., (PHENIX Collaboration), High transverse momentum η meson production in p+p,

d+Au, and Au+Au collisions at $\sqrt{s_{NN}}$ = 200 GeV. Phys. Rev. C **75**, 024909 (2007). https://doi.org/10.1103/PhysRevC.75.024909
32. L. Adamczyk, J.K. Adkins, G. Agakishiev et al., (STAR Collaboration), Energy dependence of acceptance-corrected dielectron excess mass spectrum at mid-rapidity in Au+Au collisions at $\sqrt{s_{NN}}$ = 19.6 and 200 GeV. Phys. Lett. B **750**, 64–71 (2015). https://doi.org/10.1016/j.physletb.2015.08.044
33. G. Agakichiev, H. Appelshauser, J. Bielcikova et al., (CERES Collaboration), e^+e^--pair production in Pb-Au collisions at 158 GeV per nucleon. Eur. Phys. J. C **41**, 475–513 (2005). https://doi.org/10.1140/epjc/s2005-02272-3
34. A. Adare, S. Afanasiev, C. Aidala et al., (PHENIX Collaboration), Centrality dependence of low-momentum direct-photon production in Au+Au collisions at $\sqrt{s_{NN}}$ = 200 GeV. Phys. Rev. C **91**, 064904 (2015). https://doi.org/10.1103/PhysRevC.91.064904
35. S.S. Adler, S. Afanasiev, C. Aidala et al., (PHENIX Collaboration), Measurement of direct photon production in $p+p$ collisions at $\sqrt{s}$ = 200 GeV. Phys. Rev. Lett. **98**, 012002 (2007). https://doi.org/10.1103/PhysRevLett.98.012002
36. A. Adare, S. Afanasiev, C. Aidala et al., (PHENIX Collaboration), Direct photon production in $p+p$ collisions at $\sqrt{s}$ = 200 GeV at midrapidity. Phys. Rev. D **86**, 072008 (2012). https://doi.org/10.1103/PhysRevD.86.072008
37. B.I. Abelev, M.M. Aggarwal, Z. Ahammed et al., (STAR Collaboration), Identified baryon and meson distributions at large transverse momenta from Au+Au collisions at $\sqrt{s_{NN}}$ = 200 GeV. Phys. Rev. Lett. **97**, 152301 (2006). https://doi.org/10.1103/PhysRevLett.97.152301
38. A. Adare, S. Afanasiev, C. Aidala et al., (PHENIX Collaboration), Suppression pattern of neutral pions at high transverse momentum in Au+Au collisions at $\sqrt{s_{NN}}$ = 200 GeV and constraints on medium transport coefficients. Phys. Rev. Lett. **101**, 232301 (2008). https://doi.org/10.1103/PhysRevLett.101.232301
39. A. Adare, S. Afanasiev, C. Aidala et al., (PHENIX Collaboration), Neutral pion production with respect to centrality and reaction plane in Au+Au Collisions at $\sqrt{s_{NN}}$ = 200 GeV. Phys. Rev. C **87**, 034911 (2013). https://doi.org/10.1103/PhysRevC.87.034911
40. K. Saraswat, P. Shukla, V. Singh, Transverse momentum spectra of hadrons in high energy pp and heavy ion collisions. J. Phys. Commun. **2**, 035003 (2018). https://doi.org/10.1088/2399-6528/aab00f
41. A. Adare, S. Afanasiev, C. Aidala et al., (PHENIX Collaboration), Transverse momentum dependence of η meson suppression in Au+Au collisions at $\sqrt{s_{NN}}$ = 200 GeV. Phys. Rev. C **82**, 011902 (2010). https://doi.org/10.1103/PhysRevC.82.011902
42. L. Adamczyk, J.K. Adkins, G. Agakishiev et al., (STAR Collaboration), Direct virtual photon production in Au+Au collisions at $\sqrt{s_{NN}}$ = 200 GeV. Phys. Lett. B **770**, 451–458 (2017). https://doi.org/10.1016/j.physletb.2017.04.050
43. A. Adare, S. Afanasiev, C. Aidala et al., (PHENIX Collaboration), Enhanced production of direct photons in Au+Au collisions at $\sqrt{s_{NN}}$ = 200 GeV and implications for the initial temperature. Phys. Rev. Lett. **104**, 132301 (2010). https://doi.org/10.1103/PhysRevLett.104.132301
44. L. Adamczyk, J.K. Adkins, G. Agakishiev et al., (STAR Collaboration), Elliptic flow of electrons from heavy-flavor hadron decays in Au+Au collisions at $\sqrt{s_{NN}}$ = 200, 62.4, and 39 GeV. Phys. Rev. C **95**, 034907 (2017). https://doi.org/10.1103/PhysRevC.95.034907
45. Studying the Phase Diagram of QCD Matter at RHIC. https://drupal.star.bnl.gov/STAR/files/BES_WPII_ver6.9_Cover.pdf